Effects of texturing the rake surfaces of cemented tungsten carbide tools by ultrashort laser pulses in machining of martensitic stainless steel

Article *in* International Journal of Advanced Manufacturing Technology · July 2018

DOI: 10.1007/s00170-018-2407-x

CITATIONS
0

READS
58

7 authors, including:

Alisson Machado
Pontifícia Universidade Católica do Paraná (PUC-PR)
116 PUBLICATIONS **1,944** CITATIONS

SEE PROFILE

Ricardo Elgul Samad
Instituto de Pesquisas Energéticas e Nucleares
110 PUBLICATIONS **550** CITATIONS

SEE PROFILE

The International Journal of Advanced Manufacturing Technology
https://doi.org/10.1007/s00170-018-2407-x

ORIGINAL ARTICLE

Effects of texturing the rake surfaces of cemented tungsten carbide tools by ultrashort laser pulses in machining of martensitic stainless steel

M. Bertolete[1,2] · P. A. Barbosa[2,3] · Á. R. Machado[4,5] · R. E. Samad[2] · N. D. Vieira Jr[2] · R. Vilar[6] · W. de Rossi[2]

Received: 13 February 2018 / Accepted: 9 July 2018

Abstract
The present study investigates the effect of texturing the rake face of uncoated cemented tungsten carbide tools by ultrashort laser pulses for tribological improvement. In this sense, four parallel micro-groove texturing patterns were created on the rake face of the cutting tools, beginning at a variable distance from the cutting edge. The pitch between grooves was also varied. Friction force, machining force, chip features, and surface roughness were evaluated from semi-orthogonal dry turning in the reference (non-textured) and textured tools. The results showed friction force reduction by nearly 40%; chip deformation decrease around 21%; machining force reduction by 20%; and surface roughness by 46 and 28% for Ra and Rz, respectively, for the best texturing pattern.

Keywords Texturing · Ultrashort laser pulses · Friction force · Machining force · Chip features · Surface roughness

1 Introduction

Ultrashort lasers available in conventional research laboratories are systems that can easily generate light pulses lasting from femtoseconds (10^{-15} s) to picoseconds (10^{-12} s), with energies up to hundreds of microjoules and high intensities in the 10^{12}–10^{14} W/cm^2 range. Gamaly et al. [1] describe that the very brief duration of these pulses induces nonlinear processes that transform materials that are non-resonant with their wavelength into absorbing ones. Furthermore, the pulses are shorter than the typical thermal vibration period of the lattice of solids (10^{-11}–10^{-10} s), which minimizes the energy transferred to the material. When machining with ultrashort pulses, this implies a negligible heat-affected zone, preservation of the surrounding material properties, highly precise and nonselective ablation of the matter. According to Diels and Rudolph [2], machining with ultrashort laser pulses allows etching and cutting all kinds of materials in a nanometric to micrometric precise scale. In addition, Nolte et al. [3] and Astakhov [4] pointed out that a better surface integrity is obtained with femtosecond lasers than with nanosecond or picosecond lasers.

Because of the positive response of ultrashort lasers to micromachining any kind of material, laser surface texturing (LST) emerges as a promising application of this technology. Kawasegi et al. [5] and Xing et al. [6] mention that LST allows changing the tribological, optical, mechanical, biochemical properties of the material surface, among others. In machining processes, LST has been employed experimentally for improving coating adherence. Neves et al. [7] textured HSS drills with Q-switched Nd:YAG laser with pulse length above a hundred nanosecond to improve the TiN coating adherence. Their results showed a large tool life increase for textured tools due to a better coating adhesion. Deng et al. [8] carried out nanotextures by femtosecond laser on the rake face of carbide tools and then deposited solid lubricant coating (WS_2). Their results showed better performance of the textured-coated tools than the conventional ones. LST has also been used to decrease the machining force, friction, temperature, tool wear, surface roughness,

✉ M. Bertolete
bertolete@sc.usp.br

1 Escola de Engenharia de São Carlos, Departamento de Engenharia de Produção, Universidade de São Paulo, Trabalhador São Carlense Av., 400, São Carlos, SP 13566-590, Brazil

2 Centro de Lasers e Aplicações, Instituto de Pesquisas Energéticas e Nucleares, São Paulo 05508-000, Brazil

3 Departamento de Engenharia Mecânica, Universidade Federal do Espírito Santo, Vitória 29075-910, Brazil

4 Faculdade de Engenharia Mecânica, Universidade Federal de Uberlândia, Uberlândia 38408-902, Brazil

5 Programa de Graduação em Engenharia Mecânica, Pontifícia Universidade Católica do Paraná, Curitiba 80215-901, Brazil

6 Instituto Superior Técnico, Universidade de Lisboa, 1049-001 Lisbon, Portugal

Published online: 18 July 2018

and for serving as cutting fluid reservoir, mainly when applied on the rake surface of cutting tools. Sugihara and Enomoto [9] produced nano/microtextures on the rake face of cemented carbide tools by femtosecond laser before coating them with DLC. They carried out face-milling tests in dry and wet conditions on aluminum alloy and observed a decrease in the adhesion area and friction for textured tools, associating the results to cutting fluid retention. Xie et al. [10] produced microgrooves on the rake face of cemented carbide by grinding using a diamond wheel. They tested them in turning of titanium alloy in dry condition and observed that the texture can contribute to decrease cutting temperature, force, and tool wear. Tribological tests on textured surfaces confirm the improvement, although the results depend on the form, dimension, and shaping of the textures as reported by Segu et al. [11] and Shum et al. [12].

Texturing technology application in metal cutting requires knowledge of machining fundamentals [13] as well as of the wear mechanisms from tribology [14]. In machining, the tribological details occurring at the chip-tool interface are not completely understood yet, although those phenomena are frequently quoted in the classical literature [15, 16]. The reasons for many doubts still remaining in this area are the difficulties encountered to experimentally access the chip-tool interface. The deformed chip thickness (h'); the chip thickness ratio (r), which is the ratio between undeformed (h) and deformed chip thickness (h'); and the shear plane angle (ϕ), which is the angle between the direction of the cutting speed and the primary shear plane, are valuable indicators for identifying the amount of plastic deformation involved in machining. These parameters are influenced by the friction process between the chip and the tool, being important to thoroughly understand it also from the tool resistance point of view. As the amount of plastic deformation and heat generation are very high at the chip-tool interface, a secondary shear plane is formed in this place, creating a flow zone within the chip. Data from Kawasegi et al. [5] and Sugihara and Enomoto [9] suggest that tribological features are changed at the chip-tool interface when the rake face is textured.

Most of the literature deals with texturing to modify tribological properties uses nanosecond lasers [6, 17]. However, these longer pulses inevitably produce a heat-affected zone and a layer of molten and resolidified material with debris in the processed area. The use of pulses with durations of tens or hundreds of femtoseconds may minimize, or virtually eliminate, these effects, leaving the processed surface with almost unchanged physical and mechanical characteristics.

Therefore, the aim of this work is to study the effects of texturing the rake face of uncoated cemented tungsten carbide tools by ultrashort laser pulses in machining martensitic stainless steel. For this purpose, four similar texture models were produced, varying the distance of textures from the cutting edge and the grooves' pitch. The friction force, machining force, chip features, and surface roughness were evaluated for non-textured and textured tools.

2 Materials and methods

Surface texturing was carried out on the rake face (A_γ) of triangular uncoated cemented tungsten carbide tools, BA55 (manufactured by Brassinter), using ultrashort pulses from a Ti/Sapphire laser model Femtopower Compact Pro HR/HP (Femtolasers). The 30 fs pulses were centered at 785 nm with 40 nm of bandwidth, in a pulse train with 4 kHz repetition rate and energy set at 15 μJ. The laser beam was focused on the tool surfaces by a 38-mm focal length lens. The focus spot size ($\varnothing_f$) was around 11 μm, calculated by Eq. (1) [18], where M^2 is the beam quality factor, f is the focus length, λ is the laser wavelength, and $\varnothing_0$ is the beam diameter at the lens entrance. In this case, the beam quality and the beam diameter before the lens was 2 and 7 μm, respectively:

$$\varnothing_f = \frac{4M^2 f\lambda}{\pi\phi_o} \tag{1}$$

The laser beam was plane polarized perpendicularly to the groove, and no shrouding gas was used. Figure 1 shows the laser apparatus, highlighting the amplifier, nozzle with focusing lens, CNC stage to support the samples, and micrometer for vertical manual adjustment.

The texture design comes from a previous study [19], in which a specific contact area between the chip and the tool, called sticking (or seizure) zone, was determined. At that time, the main cutting force was also measured for the tool-workpiece pair. From the literature [20, 21], it was possible to estimate the rupture strength of the tool material. Thus, from the elemental equation, $\sigma = F/A$ (stress equals force divided by the actuating area), the critical area was determined to support the load without reaching the tool material rupture strength. Knowing that the sticking area is bigger than the critical one, the proposal was to put as much grooves as possible in the chip-tool contact area, without causing the catastrophic failure of the cutting tools, and therewith disturbing the sticking and sliding zones on the rake face of the tool during machining.

In order to study the effects of texturing on the rake face, four texture models (Table 1) were proposed with grooves micro-cut parallel to the main cutting edge of the tool, starting in distances from it of 100, 200, 300, and 400 μm. The pitches of the grooves were 95, 65, 60, and 60 μm, respectively. The laser beam scanned the sample surface to generate grooves with depth and width desired in a single pass with velocity of 3 mm/min. The ablation area was 2.5 mm^2 (2.5 mm in the direction of the depth of cut and 1 mm in the feed direction).

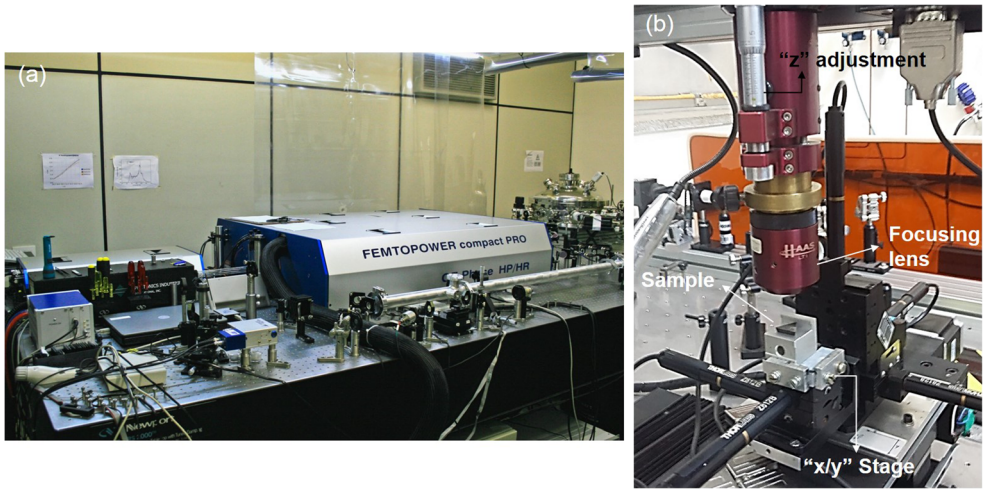

Fig. 1 Laser apparatus. **a** Ti/sapphire laser amplifier. **b** Texturing experimental arrangement

The microscopic and dimensional characterization of the textures (width and depth) were performed by a scanning electronic microscope (SEM), TM3000 (Hitachi), equipped with an energy-dispersive spectrometer (EDS), Quantax 70 (Bruker), and a 3D optical profiler, ZeGage (Zygo).

Dry machining tests were carried out with textured and non-textured (flat surface used as reference) cemented tungsten carbide inserts, P30/P40 grade (ISO), with the geometry TPUN 160304, mounted on a CTGPR 2525 M16 tool-holder both manufactured by Sandvik, allowing a semi-orthogonal cutting geometry with 0° of cutting edge inclination angle (λ_s), 11° of clearance angle (α), 6° of rake angle (γ), and 91° of cutting edge angle (k_r). A conventional lathe, S-30 (Romi), with 8 HP and 1800 rpm, was used to perform the tests. The cutting parameters were kept constant in $v_c = 156$ m/min (cutting speed), $f = 0.205$ mm/rev (feed rate), $a_p = 2$ mm (depth of cut), and $Lf = 10$ mm (feed length). These are conditions indicated by the tool manufacturer for roughing passes. The workpiece material was a martensitic stainless steel, VSM13 (Villares Metals), with an average hardness of 274 HV30, similar to UNS S41000. The chemical composition obtained by an X-ray fluorescence, Axios Advanced (PANalytical), is shown in Table 2.

The machining test output variables were the three orthogonal force components acting on the cutting tool (Fc = cutting force, Ff = feed force, and Fr = radial force), chip features, and surface roughness. According to Trent and Wright [13] and Shaw [15], from the cutting forces components and tool geometry, it is possible to calculate the friction force (Ft), tangential to the rake face in the chip exit direction, and the resulting machining force (F_R), using Eqs. (2) and (3), respectively. The orthogonal force components were monitored with the aid of a piezoelectric dynamometer model 9265B/9441B, a signal amplifier 5070A 11100, and the acquisition software DynoWare 2825A1-2 (all manufactured by Kistler). Figure 2 shows a schematic assembly of the acquisition force system.

The following chip features were assessed: the deformed chip thickness (h') was measured with the aid of an electronic outside micrometer with 0–25 mm measuring range, 0.001 mm resolution, ± 0.002 mm accuracy and spherical tip device (Digimess); the chip thickness ratio (r) was determined by the ratio between undeformed (h—estimated) and deformed (h'—measured) chip thicknesses, according to Eq. (4); and the shear plane angle (ϕ) was given by Eq. (5), which takes into account the chip thickness ratio (r) and the tool geometry. Finally, the surface roughness parameters Ra (arithmetic average height) and Rz (ten-point height) were measured by a roughness tester, Handysurf E-35B (Zeiss), with cut-off set at 0.8 mm, according to ISO 4288 [22], to quantify the surface finishing.

$$Ft = Fc.sin\gamma + Ff.cos\gamma \tag{2}$$

$$F_R = \sqrt{Fc^2 + Ff^2 + Fr^2} \tag{3}$$

$$r = \frac{h}{h'} \tag{4}$$

Table 1 Definition of texture models

Models	Cutting edge distance [μm]	Pitch [μm]
1	100	95
2	200	65
3	300	60
4	400	60

Table 2 Percentage of the main chemical elements of the VSM13 steel [wt%]

C	Cr	Fe	Mn	Si
0.12	12.30	86.30	0.53	0.35

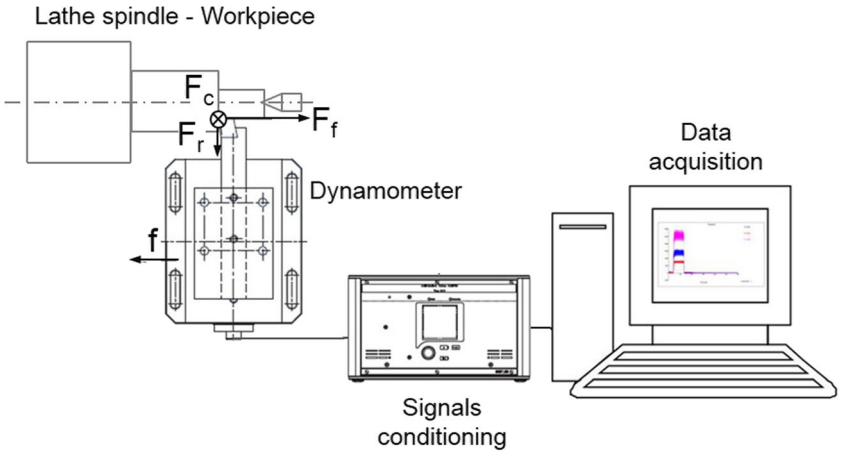

Fig. 2 Assembly of the acquisition force system

h is estimated as $h = f.sink_r$.

$$\varnothing = \tan^{-1}\left[\frac{r.cos\gamma}{1-r.sin\gamma}\right] \quad (5)$$

Although the normal force (F_N) and coefficient of friction (μ) could be estimated with the aid of the dynamometric system—$F_N = Fc.cos\gamma–Ff.sin\gamma$ and $\mu = Ft/F_N$—in most metal cutting conditions, the classical friction approach is inappropriate. According to Hutchings [14], in the first friction law, μ is dependent on F_N and Ft but independent of the contact area; the normal stress is much smaller than the yield stress of soft material. In this case, the real contact area is very small in comparison to the apparent one, and contacts only occur at the top of the peaks. In machining, Trent and Wright [13] state that in the sticking (or seizure) zone, the two surfaces (chip and tool) are completely in contact with the normal stress exceeding the yield stress; the real area of contact becomes independent of F_N; and Ft is the force required to shear the material across the interface, which is proportional to the contact area.

3 Results and discussions

Texture characterization is firstly presented to specify the patterns and their dimensions. Next, the machining results will be presented, allowing comparisons between textured and non-textured tools through the output variables.

3.1 Texture characterization

Figure 3 shows the four texture models created by the ultrashort pulses varying both the distance from the cutting edge and the pitch of the grooves.

To machine the texture grooves, the process parameters were chosen to minimize possible collateral damage effects such as melting and excessive deepening in the center of the grooves. The 15.8 J/cm^2 fluence used is well above the ablation threshold for a large number of overlapped pulses, to be $F_{th,\infty} \sim 0.08$ J/cm^2, measured by the D-scan method [23], but low enough to etch shallow grooves that do not affect (weaken) the tool structure.

To evaluate the effects of the ultrashort pulses machining, SEM micrographies of the etched grooves were acquired with magnifications above × 1000, and Fig. 4 shows a representative image obtained.

Although the pulse energy and focusing were such as to ensure that the ablation occurred in the high-fluence regime, with material being removed by phase-explosion and spallation [1], no trace of molten material or other kinds of flaws, such as cracks or spalling, were found on the machined surface. Due to the low energies used (a few microjoules), any residual thermal effect on the vicinity of the groove is reduced to a very small region and could not be observed in the micrometer scale. The Gaussian profile of the spatial energy distribution, which would be perpendicular to the image plane, causes a further deepening in the center line of the groove, leading to a "v"-shaped profile of the machined region, where in the border, the energy is much lower with minimal ablation effect. This is confirmed by the substrate grain structure on the outer edge of the groove, in which preserved WC grains (lighter gray tone) can be seen. Additionally, laser-induced periodic surface structures (LIPSSs), which are nanometric textures generated in the low fluence regime [24], can be observed at the grooves borders, where the laser intensity drops quickly. These LIPSSs have very small influence on the tool strength and also emphasize the metallic characteristic of the material. These results are clearly superior to those obtained when machining similar materials with nanosecond pulses, in which thermal effects that dominate the ablation process [25] promote melting and phase transitions in the substrate. These effects can be seen in Zhang et al. [17], in which 10-ns pulses from a Nd:YAG laser at 5000 Hz with scanning velocity of 20 mm/

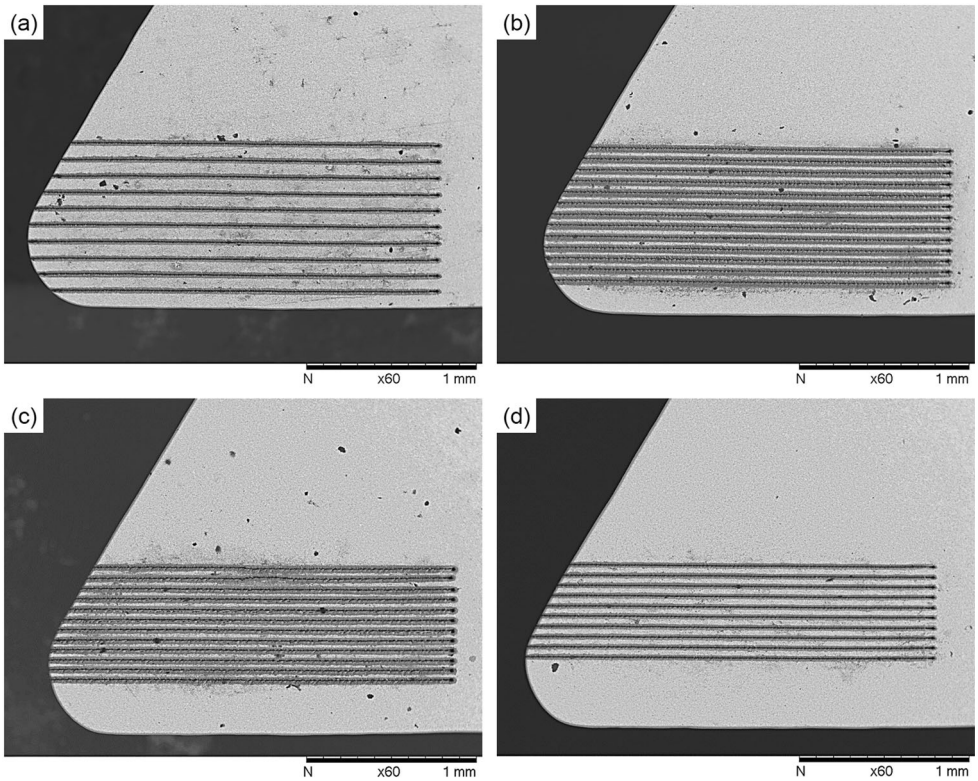

Fig. 3 SEM characterization of texture models from the cutting edge. **a** At 100 μm with 95 μm pitch. **b** At 200 μm with 65 μm pitch. **c** At 300 μm with 60 μm pitch. **d** At 400 μm with 60 μm pitch

s were used to etch the rake face of a WC-Co tool to produce linear and parallel microgrooves in v form with depth and width dimensions of 50 μm. In that work, molten and resolidified material with debris can be observed. This comparison reinforces the advantage of ultrashort laser pulses, as quoted in the literature [26, 27], which is the ability to minimize the thermal effects during micromachining, due to their brief duration, and preserve the substrate properties. This may be critical when LST is applied to cutting tools with high hardness/toughness ratio, such as ceramic tools, whereby large damages at the microstructure may lead to a catastrophic failure.

Figure 5 shows an image of the optical profiler for the texture model 300 μm away from the cutting edge. This is a representative image of the shape and dimension of the grooves obtained, since the laser parameters were kept constant for all patterns. The profile characterization allowed evaluating the v form of the grooves produced and their reproducibility regarding their width and depth.

Table 3 presents the mean values of the width and depth of the grooves for each texture model fabricated; besides, the averages of all width and depth values are given for comparison (global averages). The width of the grooves has an average value of 35.2 μm, while the depth, an average value of

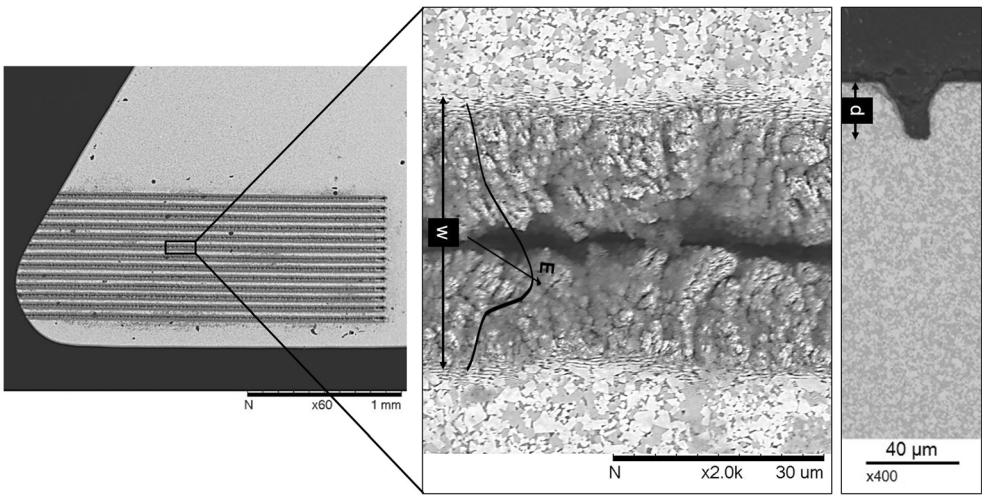

Fig. 4 SEM image of one groove to evaluate the machining effects by ultrashort pulses (w = width, d = depth, and E = energy)

32.0 μm. The latter has a larger standard deviation than the former, probably due to the laser intensity variations caused by the plasma formed at the focus. The standard deviations of the table are observed to be rather small, including the global average. According to Kawasegi et al. [5] and Samad and Vieira [28], ultrashort pulse lasers provide micromachining with very accurate dimensions, which are associated to the CNC table precision and the non-thermal and highly nonlinear character of the ultrashort pulses ablation, which defines a precise ablation threshold that is spatially localized.

3.2 Machining test results

Practical machining results comparing the performance of textured tools and non-textured ones (reference) are presented next. Figure 6 shows average values of the friction force (*Ft*) on the rake face of the tools. For the reference tool, the value obtained was (1294 ± 87) N. The texture model with the best result, tool textured at 300 μm from the cutting edge, presented a friction force of (779 ± 48) N, a reduction of 40%. Note that there is a decrease in *Ft* up to the 300-μm texture pattern and, after that, *Ft* increases again. Similar results were found by Obikawa et al. [29] with microtextured cemented carbide tools made by chemical etch when machining an aluminum alloy under lubricate condition. Considering the Bowden and Tabor model for sliding friction, which assumes the friction force as the resultant from the adhesion and deformation forces [14], the results of friction forces suggest that a large adhesion of the workpiece material is occurring on the rake face, leading to an increase in the contact area (junction growth) and a higher plastic strain in the chip when machining with the reference tool. According to that, any factor that affects the chip movement on the rake face will cause changes in the size of the shear plane areas, and thus in the machining

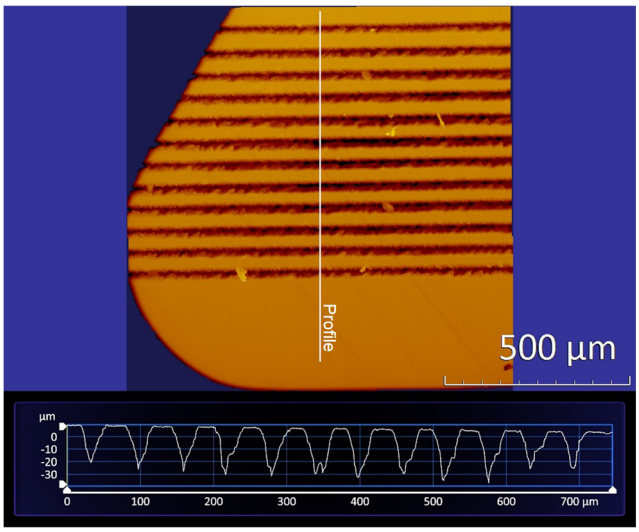

Fig. 5 3D optical profile of the texture of a tool showing shape and dimensional features

force, chip features, cutting temperature, and tool wear. Some of these topics will be discussed later.

Figures 7 and 8 show images of the rake face of the tools after machining, with evidences of work material adhered that influenced the friction force. Figure 7a suggests the division of the chip-tool contact area for the reference tool in the sticking zone (dashed line), where the real area of contact is equal to the apparent one, and the sliding zone (limited by the continuous line), where the intermittent contact predominates, i.e., stick-slip conditions. Adhered work material close to the cutting edge can be observed with strong traces of material flow from the border of this zone. The figure shows a contact length from the cutting edge of around 2 mm in the vertical direction, larger than those encountered in the textured tools. For the latter, the distance from the cutting edge up to the last groove is 1 mm and the chip-tool contact area does not seem to extend beyond it, as can be observed in Fig. 8. If *Ft* is proportional to the contact area and this decreases in textured tools, the behavior of the *Ft* curve is explained. As the shear plane areas are changing in textured tools, the machining force components are also expected to be influenced. It is worth stressing that the sticking zone length for the reference tool is around 533 μm; this cannot be stated for the textured tools because the division of the chip-tool contact area is not clear. Figure 7b shows an EDS analysis with evidence of the workpiece material (iron and chromium) adhered to the rake face of the cemented carbide tool, and the same analysis can be observed in Fig. 8.

There is metallic bonding between the work material and the cutting tool on the rake face because the chip is subjected to a huge plastic strain during its formation, due to high compressive and shear stresses, which imply temperature rise. However, the relative movement occurs under conditions of seizure because the sticking area is small and there is sufficient force applied to shear the work material at the chip-tool interface; the flow of metal on the rake face thus sweeps away any contaminants that could prevent or minimize adherence. Therefore, during chip formation, the conditions strongly favor metallic bonding at the interface [13].

Deformation forces from the friction theory may be related to chip plastic strain. Table 4 shows the deformed chip thickness (h'), the chip thickness ratio (r), and the shear plane angle (ϕ), which provides information about the amount of deformed material during chip formation.

The textured tools present lower chip thickness, higher chip thickness ratio, and higher shear plane angle than the reference tool. Therefore, textured tools produce less deformed chips; consequently, the size of the shear plane areas are smaller, indicating that the cutting temperature is lower, which might affect the tool wear resistance, since elevated temperatures accelerate the wear mechanisms. The wear mechanisms in cemented carbide or ceramic textured cutting tools can involve brittle fracture, tribochemical effects, and plastic flow

Table 3 Average values of the width and depth of the grooves

	Average values [μm]				
	100 μm	200 μm	300 μm	400 μm	Global average [μm]
Width	29.7 ± 1.3	37.0 ± 1.0	37.0 ± 1.3	36.2 ± 1.9	35.2 ± 3.2
Depth	30.1 ± 4.0	33.7 ± 7.5	33.9 ± 4.3	29.3 ± 5.2	32.0 ± 5.7

with fatigue and fragments being removed by adhesive processes (attrition). However, preliminary tests show an increase in the textured tool life, as opposed to the non-textured one, as observed by other researchers [6, 17]. The results for textured tools do not allow stating that the tool with 300 μm texture pattern produced the least deformed chip, because the standard deviations make these values too close. However, note that the further the texture starts away from the cutting edge, the closer the tool is to the original form (non-texture), as with the 400 μm pattern. Furthermore, the average value of the chip thickness ratio of the textured tools, including the 400 μm texture model, is around 21% higher than for the chip produced with the reference tool, indicating lower deformation.

The results quoted above are also supported by the literature. Sugihara and Enomoto [9] produced nano/microtextured cemented cutting tools, coated with DLC and applied them to milling aluminum in wet conditions. The authors observed greater shear plane angles for nano/microtextured tools than for non-textured ones. Kawasegi et al. [5] also observed greater variation in the shear angle for nanotextured cemented carbide tools as compared to non-textured one, when turning an aluminum alloy with minimum quantity lubrication. Xie et al. [10] microtextured non-coated cemented carbide tools and observed a gradual increase in the shear plane angle until an optimum point was reached, when the micro-groove depth and pitch varied in a range from 7 to 149 μm and 50 to 300 μm, respectively. They related the shear plane angle with the cutting temperature, observing that the lowest temperature occurred exactly for the highest angle (optimum point).

So far, it is not clear why the texture on the tools decreases deformation (deformation forces) and adhesion (adhesion forces) in machining. As discussed previously, during machining, chip formation occurs under a high level of plastic strain. Initially, oxides can contaminate the rake face of the cutting tool, but the shearing process (force) sweeps the contaminants away and a flow zone takes place in the chip-tool interface, where no gap at all can be seen. The metal flows across a clean rake face without access of any sort of gas from the atmosphere, making contact with the rake face at elevated temperatures, which increases the ductility of the deformed material and favors strong adhesion. Figure 7 showed a larger contact area on the reference tool as compared to the textured ones (Fig. 8). Tribofilm formation is believed to occur in textured tools due to the very high compressive stress, helping chip material to adhere to the grooves of the rake face (hard counterface), thus facilitating the formation of the flow zone. This changes the frictional behavior and, as suggested by Hutchings [14], may result in re-orientation of the surface crystalline structure in a way that reduces the frictional force. Figure 9a shows workpiece material anchored in the grooves on the rake face of a textured tool. Note that this adherent material has traces of shearing in the direction of the chip movement. When compared with the rake face of the reference tool (Fig. 9b), the thickness of the adhered material on the textured tool seems to be thicker. This indicates that thinner films on the chip-tool interface (reference tool condition) do not necessarily mean a drop in friction, but on the contrary, a larger contact area with the seizure zone and a greater sliding zone with more asperities in contact with the chip is intensely present. However, there may be an optimum texture condition to promote lower friction at the chip-tool interface due to the film thickness and/or the position of the texture in relation to the sticking and sliding zones. This situation is similar to the condition of sliding a soft metal layer on a harder surface (solid lubrication). Studies in this direction give room for further investigation, when different texture patterns should be tried taking into account film thickness and position of the texture. From the tribology literature, such phenomenon can be explained as the clogging effect that can happen when smearing a soft material with sand papers. Goddard and Wilman [30] and Bijwe et al. [31] pointed out the worn off material clogs the spaces among the abrasives decreasing friction, load, wear rate, and abrasivity. Gåhlin and Jacobson [32] used the clogging effect to explain abrasive particle size effect in abrasion. The authors manufactured ideally abrasive particles by micromechanical etching techniques with different packing density and size (fine, medium, and coarse grains). They observed a significant reduction in the wear rate for the fine particle size due to the clogging effect of abrasives by this softer workpiece material.

Figure 10 shows the machining force results for the tested tools. The pattern of the curves are similar to the friction force ones (Fig. 6). The machining forces for all the textured tools are lower than those produced by the reference tool. This ratifies the previous discussion, the results of which suggest the existence of an optimal texture condition that might lead to a minimum machining force. The explanation for the decrease in forces can be associated to the tribological changes in the tool-chip interface (clogging effect) causing the reduction of the primary and secondary shear planes during chip formation.

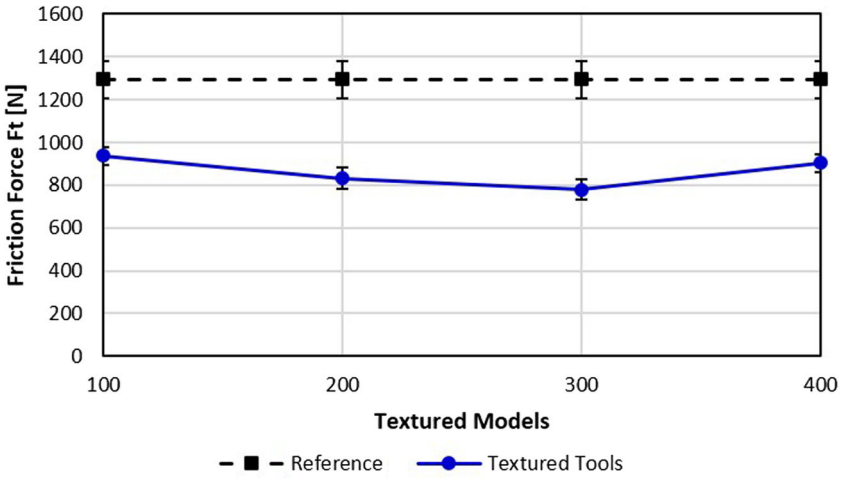

Fig. 6 Friction force results

With the tools tested, the best performance was obtained by the 300-μm texture model which promoted a 21% reduction in the machining force. This result is mainly caused by the influence of *Fc* and *Ff*, which showed 9 and 44% reduction, respectively. These are important results, allowing considering that textured tools by ultrashort laser pulses are an interesting alternative since a great reduction in the cutting loads is expected. According to the present results, at least 9% decrease in power consumption obtained for the 300-μm texture model implies energy saving and higher efficiency, i.e., driving towards sustainability.

The results corroborate those found in the literature in different tribological conditions. Kawasegi et al. [5] textured cemented carbide tools by ultrashort pulses in the nano- and microscale ranges. The authors studied the tool performance when turning an aluminum alloy (A5052) in finishing cutting conditions ($v_c = 600$ m/min; $f = 0.1$ mm/rev; and $a_p = 0.2$ mm), using minimum quantity lubrication (MQL). Their results indicated a more effective reduction in the *Ff* and *Fr* components than in the *Fc* ones, when the latter presented only a small advantage for the nanotextured tools. They also found adherence of workpiece material on the rake face of the tools. Xie et al. [10] textured cemented carbide tools, varying the depth and width of the grooves in a microscale range, using a diamond wheel. They tested these tools in turning a titanium alloy (Ti-6Al-4V) in finishing ($v_c = 47$–49 m/min; $f = 0.1$ mm/rev; and $a_p = 0.5$ mm) and medium conditions ($v_c = 39$ m/min; $f = 0.3$ mm/rev; and $a_p = 1$ mm), both in dry cutting. They found a great reduction in *Fc*, a considerable reduction in the cutting temperature and less chip deformation for the textured tools as compared to the non-textured ones. Zhang et al. [17] textured cemented carbide tools in a microscale range with nanosecond pulses from a Nd:YAG laser and coated them with TiNAl. The authors tested these tools for machining AISI 1045 hardened steel in finishing turning conditions (f = 0.1 mm/rev and $a_p = 0.3$ mm), in dry and lubricated atmospheres. The most interesting results derived from $v_c =$ 200 m/min, when *Fr*, *Ff*, and *Fc* decreased by 33, 34.7, and 21.2%, respectively, in lubricated condition; whereas in dry condition, the cutting force reduction was 2–8% as compared with the non-textured tools. The authors also observed workpiece material adhered at $v_c = 160$ m/min, and more cutting

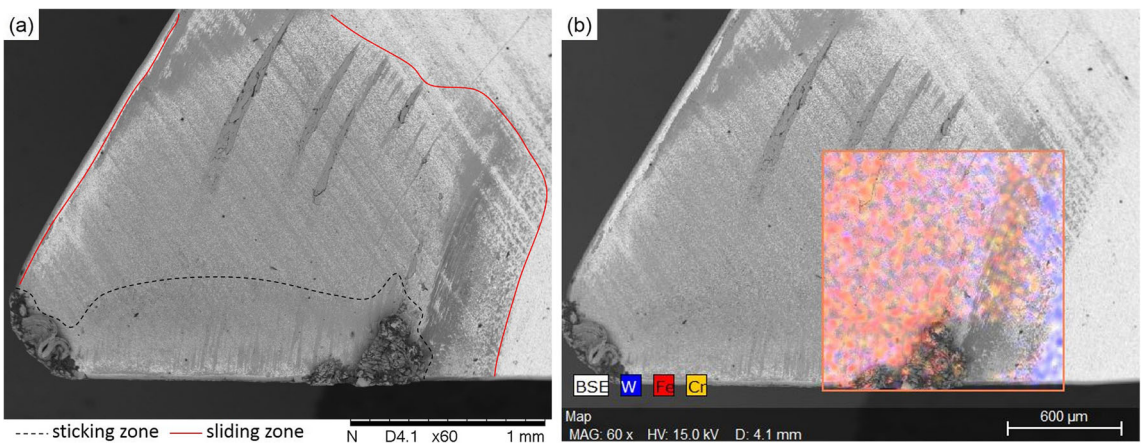

Fig. 7 Chip-tool contact area for the reference tool. **a** Suggested delineation of the sticking (dashed line) and sliding (continuous line) zones. **b** EDS analysis

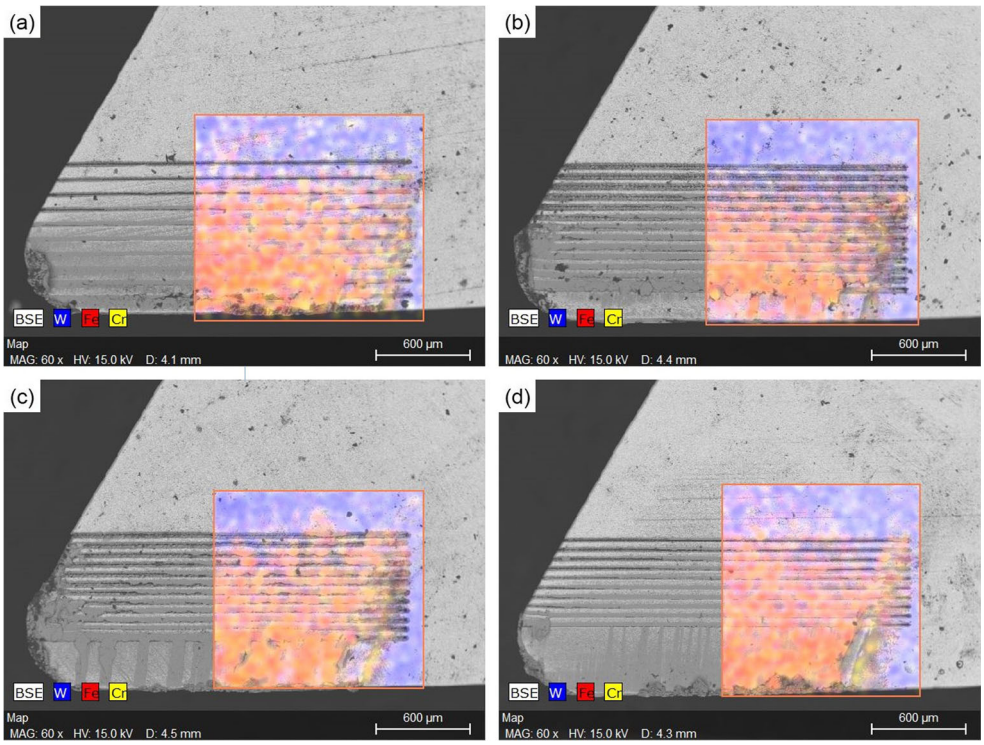

Fig. 8 Rake face of the textured tools with EDS analysis. **a** At 100 µm. **b** At 200 µm. **c** At 300 µm. **d** At 400 µm

fluid chemical element was detected on the rake face of the textured tools. Besides, lower tool wear was observed in the textured tools than in non-textured ones, be it in lubricated or dry condition. Barbosa et al. [19] microtextured cemented carbide tools with four different models, varying the texture distance from the cutting edge and the pitch between grooves. The authors experimented them in dry turning an austenitic stainless steel (AISI 304UF) using the following cutting conditions: $v_c = 160$ m/min, $f = 0.2$ mm/rev, and $a_p = 2.0$ mm. They found lower machining force values for the textured tools than for the non-textured one. In the best texture condition tested, there was a 28% reduction in the machining force and assigned this result to the workpiece material anchored in the microgrooves.

Tribological tests also confirm that there is a dependence on dimension and density of texture, which cause tribological behavior changes able to decrease friction and wear. Shum et al. [12] carried out laser surface texturing (Nd:YAG laser) on M2 high-speed steel to improve the wear resistance of a DLC coating, applied after the laser surface treatment. The authors varied the density and diameter of dimples. They observed an optimization tendency for appropriate density and dimension of dimples with a 20% reduction in friction and nearly 52% in wear rate, during reciprocating sliding-wear testing under oil-lubricated condition. Segu et al. [11] studied the effect of multi-scale textures combining circular and elliptic dimples made by Nd:YAG nanosecond-pulsed laser in a pin-on-disc testing. AISI 52100 steel was the material of body and counterbody, the pins were textured, and the tests were carried out in oil lubrication regime. The authors observed the influence of dimple density on the results and found a lower coefficient of friction for the textured samples as compared to non-textured ones. Xing et al. [6] textured Si_3N_4/TiC ceramic by Nd:YAG nanosecond-pulsed laser varying the geometry and distance of grooves. They carried out a ball-on-disc reciprocating sliding test in dry condition and observed the influence of the geometry and distance of the grooves, decreasing the coefficient of friction and wear rate in comparison to the non-textured sample. Esteves et al. [33] textured cemented carbide by femtosecond laser varying the distance between microgrooves (pitch)

Table 4 Assessment of chip features

	h' [mm]	Chip thickness ratio, r [mm]	Shear plane angle, ϕ [°]
Reference	0.469 ± 0.019	0.438 ± 0.019	24.53 ± 0.96
100 µm	0.361 ± 0.013	0.569 ± 0.022	31.05 ± 1.03
200 µm	0.358 ± 0.012	0.573 ± 0.019	31.21 ± 0.92
300 µm	0.364 ± 0.007	0.564 ± 0.010	30.80 ± 0.49
400 µm	0.397 ± 0.013	0.517 ± 0.017	28.52 ± 0.83

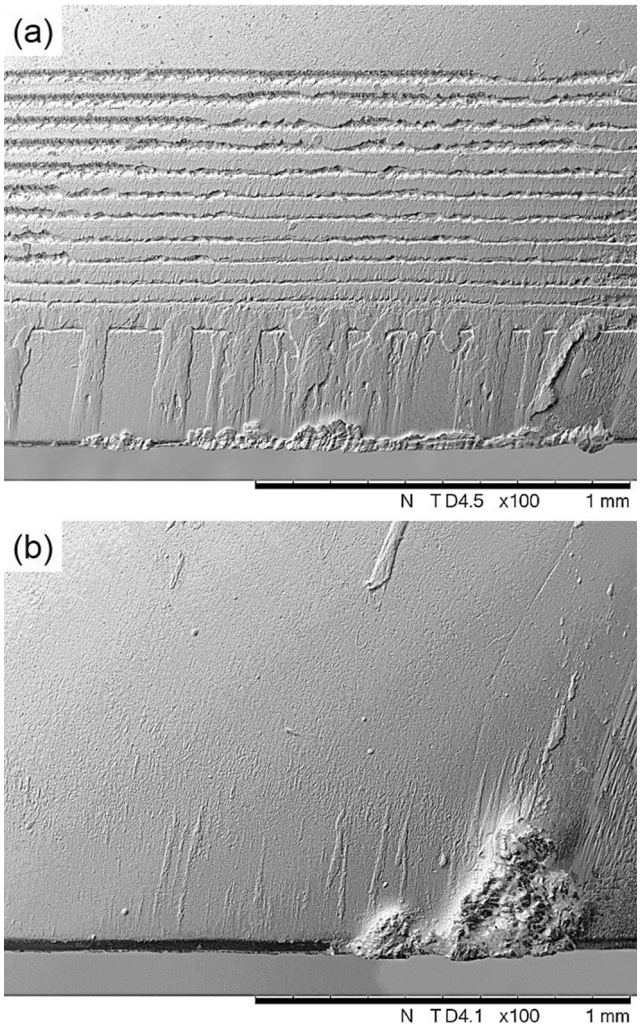

Fig. 9 Workpiece material adhered to the rake face forming a tribofilm. **a** Texture pattern at 300 μm from the cutting edge. **b** Reference tool

and valley depth. They carried out a microscale abrasion test, sphere-on-plane, with SiC slurry following the routine

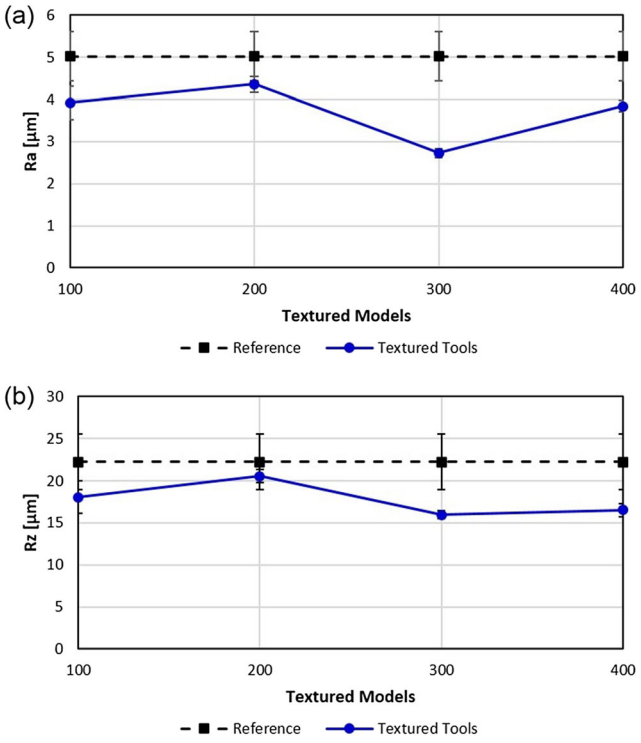

Fig. 11 Surface roughness evaluation. **a** Ra parameter. **b** Rz parameter

suggested by Rutherford and Hutchings [34] and observed a reduction in the wear coefficient by up to 25% in favor of the textured sample, as compared to the non-textured one.

Surface roughness results (Ra and Rz parameters) are presented in Fig. 11. The roughness values for the textured tools are lower than the reference ones. Again, the more pronounced results were produced by the texture model at 300 μm from the cutting edge. For Ra, the reduction was 46%, and for Rz, 28%, when compared to the surface roughness parameters given by the reference tool. These results can be explained by the *Fr* (radial force), which influence the chatter phenomenon, harming the surface finishing. This force

Fig. 10 Machining force results for the tested tools

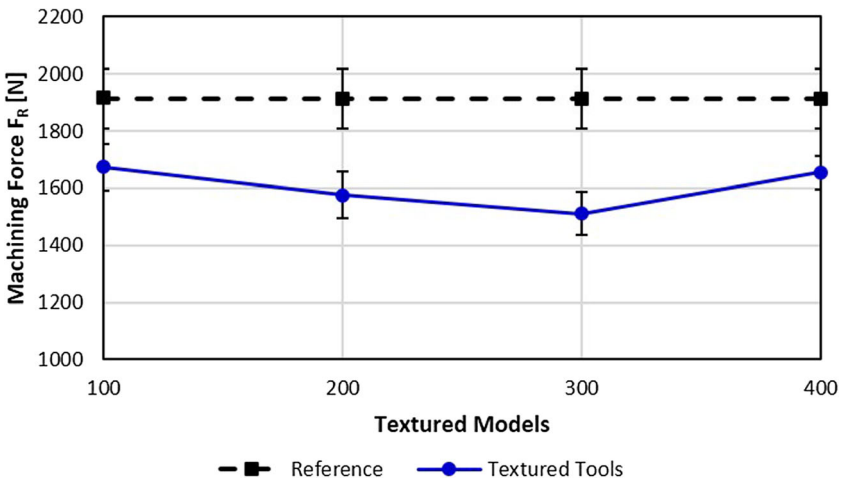

was 36% inferior for the 300-μm texture pattern in comparison to the reference one.

The surface roughness results presented are in accordance with the literature. Zhang et al. [17] noted that their microtextured cemented carbide tools provided a better surface finishing, mainly in lubricated condition, than non-textured tools. Barbosa et al. [19] also observed a reduction in the surface roughness parameters Ra and Rz, between 30 and 40% and 26 and 30%, respectively, for their models of microtextured cemented carbide tools in comparison to the non-textured one.

4 Conclusions

Cutting tool texturing by lasers, either by ultrashort on nanosecond pulses, improves their tribological performance, ultimately resulting in a machining efficiency increase.

The investigation on the effect of different texture models (varying the distance from the cutting edge and groove pitch) machined by ultrashort laser pulses on the rake face of cemented tungsten carbide tools and the comparison of the use of non-textured tool (reference tool) during the machining of VSM13 martensitic stainless steel provided interesting conclusions in favor of the textured tools. SEM images of the femtosecond laser-etched structure vicinity showed grains preserved after the cutting, no molten material on the surface, and the presence of LIPSS. These suggest a minimal heat-affected zone under the micrometric scale, maintaining the tool material properties in their surroundings. These results are superior to those from nanosecond lasers, whereby thermal processes dominate and change the etched material.

The texturing is believed to change the tribological behavior in the sliding zone, since the results showed better performance for the texture model that starts from a distance of 300 μm from the cutting edge. Tribological evidences showed that for the best model, texturing provided a drop in the friction force by nearly 40%; a decrease in chip deformation by about 21%, consequently allowing the hypothesis that the cutting temperature also drops; a reduction in the machining force by 20%; and an improvement in the surface roughness: 46% for Ra and 28% for Rz. In addition, the textures were observed to provide lower standard deviation values when compared with the reference tool.

Funding CNPq (Grants 405707/2013-4; 150490/2014-3; 150188/2015-3) and FAPESP (Grant 2013/26113-6) provided the financial support and Villares Metals donated the workpieces.

References

1. Gamaly EG, Rode AV, Luther-Davies B, Tikhonchuk VT (2002) Ablation of solids by femtosecond lasers: ablation mechanism and ablation thresholds for metals and dielectrics. Phys Plasmas 9:949–957. https://doi.org/10.1063/1.1447555
2. Diels J-C, Rudolph W (2006) Ultrashort laser pulse phenomena: fundamentals, techniques, and applications on a femtosecond time scale, 2 nd. Elsevier/Academic Press, New York
3. Nolte S, Momma C, Jacobs H et al (1997) Ablation of metals by ultrashort laser pulses. J Opt Soc Am B 14:2716. https://doi.org/10.1364/JOSAB.14.002716
4. Astakhov VP (2014) Drills : science and technology of advanced operations. CRC Press, New York
5. Kawasegi N, Sugimori H, Morimoto H et al (2009) Development of cutting tools with microscale and nanoscale textures to improve frictional behavior. Precis Eng 33:248–254. https://doi.org/10.1016/j.precisioneng.2008.07.005
6. Xing Y, Deng J, Feng X, Yu S (2013) Effect of laser surface texturing on Si3N4/TiC ceramic sliding against steel under dry friction. Mater Des 52:234–245. https://doi.org/10.1016/j.matdes.2013.05.077
7. Neves D, Diniz AE, de Lima MSF (2006) Efficiency of the laser texturing on the adhesion of the coated twist drills. J Mater Process Technol 179:139–145. https://doi.org/10.1016/j.jmatprotec.2006.03.068
8. Deng J, Lian Y, Wu Z, Xing Y (2013) Performance of femtosecond laser-textured cutting tools deposited with WS2 solid lubricant coatings. Surf Coat Technol 222:135–143. https://doi.org/10.1016/j.surfcoat.2013.02.015
9. Sugihara T, Enomoto T (2009) Development of a cutting tool with a nano/micro-textured surface—improvement of anti-adhesive effect by considering the texture patterns. Precis Eng 33:425–429. https://doi.org/10.1016/j.precisioneng.2008.11.004
10. Xie J, Luo MJ, Wu KK et al (2013) Experimental study on cutting temperature and cutting force in dry turning of titanium alloy using a non-coated micro-grooved tool. Int J Mach Tools Manuf 73:25–36. https://doi.org/10.1016/j.ijmachtools.2013.05.006
11. Segu DZ, Choi SG, Hyouk CJ, Kim SS (2013) The effect of multi-scale laser textured surface on lubrication regime. Appl Surf Sci 270:58–63. https://doi.org/10.1016/j.apsusc.2012.12.068
12. Shum PW, Zhou ZF, Li KY (2013) Investigation of the tribological properties of the different textured DLC coatings under reciprocating lubricated conditions. Tribol Int 65:259–264. https://doi.org/10.1016/j.triboint.2013.01.012
13. Trent E, Wright PK (2000) Metal cutting, 4th edn. Butterworth-Heinemann, Boston
14. Hutchings IM (1992) Tribology : friction and wear of engineering materials. Arnold, London
15. Shaw MC (2005) Metal cutting principles. Oxford University Press, New York
16. Boothroyd G, Knight WA (2006) Fundamentals of machining and machine tools, 3rd edn. Taylor and Francis, New York
17. Zhang K, Deng J, Xing Y et al (2015) Effect of microscale texture on cutting performance of WC/Co-based TiAlN coated tools under different lubrication conditions. Appl Surf Sci 326:107–118. https://doi.org/10.1016/j.apsusc.2014.11.059
18. Steen WM, Mazumder J (2010) Laser material processing. Springer, London
19. Barbosa P, Bertolete M, Samad R, et al (2015) Investigation of femtosecond laser texturing in cemented carbide cutting tools. In: Lasers in manufacturing conference. Munich
20. Ezugwu EO, Pashby IR (1992) High speed milling of nickel-based superalloys. J Mater Process Technol 33:429–437. https://doi.org/10.1016/0924-0136(92)90277-Y

21. Shi XL, Shao GQ, Duan XL et al (2005) Mechanical properties, phases and microstructure of ultrafine hardmetals prepared by WC–6.29Co nanocrystalline composite powder. Mater Sci Eng A 392: 335–339. https://doi.org/10.1016/j.msea.2004.09.043
22. International Organization for Standardization (1996) ISO 4288: 1996 Geometrical Product Specifications (GPS)—surface texture: profile method—rules and procedures for the assessment of surface texture
23. Machado LM, Samad RE, de Rossi W, Junior NDV (2012) D-scan measurement of ablation threshold incubation effects for ultrashort laser pulses. Opt Express 20:4114–4123. https://doi.org/10.1364/OE.20.004114
24. Bonse J, Rosenfeld A, Krüger J (2009) On the role of surface plasmon polaritons in the formation of laser-induced periodic surface structures upon irradiation of silicon by femtosecond-laser pulses. J Appl Phys 106:104910. https://doi.org/10.1063/1.3261734
25. Stuart BC, Feit MD, Rubenchik AM et al (1995) Laser-induced damage in dielectrics with nanosecond to subpicosecond pulses. Phys Rev Lett 74:2248–2251. https://doi.org/10.1103/PhysRevLett.74.2248
26. Liang WL, Ngoi BKA, Lim LEN et al (2003) Micromachining of circular ring microstructure by femtosecond laser pulses. Opt Laser Technol 35:285–290. https://doi.org/10.1016/S0030-3992(03)00009-4
27. Wang XC, Zheng HY, Chu PL et al (2010) High quality femtosecond laser cutting of alumina substrates. Opt Lasers Eng 48:657–663. https://doi.org/10.1016/j.optlaseng.2010.02.001
28. Samad RE, Vieira ND (2006) Geometrical method for determining the surface damage threshold for femtosecond laser pulses. Laser Phys 16:336–339. https://doi.org/10.1134/S1054660X06020228
29. Obikawa T, Kamio A, Takaoka H, Osada A (2011) Micro-texture at the coated tool face for high performance cutting. Int J Mach Tools Manuf 51:966–972. https://doi.org/10.1016/j.ijmachtools.2011.08.013
30. Goddard J, Wilman H (1962) A theory of friction and wear during the abrasion of metals. Wear 5:114–135. https://doi.org/10.1016/0043-1648(62)90235-1
31. Bijwe J, Indumathi J, John Rajesh J, Fahim M (2001) Friction and wear behavior of polyetherimide composites in various wear modes. Wear 249:715–726. https://doi.org/10.1016/S0043-1648(01)00696-2
32. Gåhlin R, Jacobson S (1999) The particle size effect in abrasion studied by controlled abrasive surfaces. Wear 224:118–125. https://doi.org/10.1016/S0043-1648(98)00344-5
33. Esteves P, Bozzi A, Scandian C, et al (2015) Femtosecond laser texturing effect on abrasive wear of cemented carbide tools. In: 23rd International Congress of Mechanical Engineering (COBEM). Rio de Janeiro
34. Rutherford KL, Hutchings IM (1996) A micro-abrasive wear test, with particular application to coated systems. Surf Coat Technol 79: 231–239. https://doi.org/10.1016/0257-8972(95)02461-1